J. Cell Commun. Signal. (2018) 12:193–204
https://doi.org/10.1007/s12079-017-0430-6

RESEARCH ARTICLE

Acute connexin43 temporal and spatial expression in response to ischemic stroke

Moises Freitas-Andrade[1] · **Jennifer She**[1] · **John Bechberger**[1] · **Christian C. Naus**[1] · **Wun Chey Sin**[1]

Received: 23 October 2017 / Accepted: 25 October 2017 / Published online: 13 November 2017

Abstract Connexin43 (Cx43) gap junctions expressed in astrocytes can significantly impact neuronal survival in stroke. However, little is known regarding Cx43 spatial and temporal expression during the initial stages of brain ischemia. Using immunohistochemistry and Western blot analysis, we examined Cx43 spatial and temporal expression as a function of neuronal injury within the first 24 h after permanent middle cerebral artery occlusion (pMCAO). Western blot analysis showed a significant increase in Cx43 protein expression in the core ischemic area at 2 and 3 h after pMCAO. However, after 6 h of pMCAO Cx43 levels were significantly reduced. This reduction was due to cell death and concomitant Cx43 degradation in the expanding focal ischemic region, while the peri-infarct zone revealed intense Cx43 staining. The neuronal cell-death marker Fluoro-Jade C labeled injured neurons faintly at 1 h post-pMCAO with a time-dependent increase in both intensity and size of punctate staining. In addition, decreased microtubule-associated protein 2 (MAP2) immunoreactivity and thionin staining similarly indicated cell damage beginning at 1 h after pMCAO. Taken together, Cx43 expression is sensitive to neuronal injury and can be detected as early as 2 h post-pMCAO. These findings underscore Cx43 gap junction as a potential early target for therapeutic intervention in ischemic stroke.

Keywords Gap junctions · connexin43 · Stroke · Mouse model

Moises Freitas-Andrade and Jennifer She contributed equally to this work.

✉ Wun Chey Sin
wcsin@mail.ubc.ca

[1] Department of Cellular and Physiological Sciences, Life Sciences Institute, The University of British Columbia, 2350 Health Sciences Mall, Vancouver, BC V6T 1Z3, Canada

Abbreviations

Cx26	Connexin26
Cx30	Connexin30
Cx43	Connexin43
DAPI	4′,6-diamidino-2-phenylindole
GFAP	Glial Fibrillary Acidic Protein
MCA	Middle Cerebral Artery
pMCAO	Permanent Middle Cerebral Artery Occlusion
MAP2	Microtubule-associated protein 2
OCT	Optimal Cutting Temperature Compound
PBS	Phosphate Buffered Saline
RIPA	Radioimmunoprecipitation Assay
TBS-T	Tris-buffered saline with Tween 20

Introduction

Stroke results in inevitable cell death within the focal region, known as the ischemic core or infarct. The expansion of the ischemic core into the surrounding peri-infarct zone increases the area of damage that may occur if blood flow is not restored, either by treatment or self-recovery (Ramos-Cabrer et al. 2011). The peri-infarct is a dynamic region of low cerebral blood flow where neurons are in a critically reduced metabolic state and loss of electrical excitability. Cell survival within the peri-infarct is highly time-dependent and the treatment window is narrow. For example, tissue plasminogen activator (tPA) effectiveness drops sharply after 3–4.5 h (Lansberg et al. 2009). The search for effective therapeutic agents that impact early molecular and cellular targets within the salvageable peri-infarct is an area of intense research (Broussalis et al. 2012; George and Steinberg 2015). Connexin43 (Cx43) gap junction expression has been linked with several brain injury paradigms, including stroke (reviewed in Freitas-Andrade and Naus 2016). Moreover,

several groups have characterized pharmacological agents that specifically target Cx43 function (Yoon et al. 2010a, b; Davidson et al. 2012) and have shown significant neuroprotective benefits (Freitas-Andrade et al., Targeting MAPK phosphorylation sites of the C-terminus provides neuroprotection in stroke. submitted). However, to effectively administer treatment at the appropriate time-window, it is critical to understand the spatial and temporal expression of Cx43 during stroke onset.

Gap junctions are composed of individual connexin proteins that assemble into hexamers around a central hydrophilic pore to form transmembrane channels, termed connexons. Connexons couple with apposing connexons on neighboring cells, forming gap junctions, which coalesce into dense gap junction plaques that may contain thousands of channels (Giaume and Theis 2010). Amino acids, ions, nucleotides, and second messengers (e.g., Ca^{2+}, cAMP, cGMP, IP_3) are among the molecules that pass through gap junction channels (Barreto et al. 2011). While Cx43 gap junction plaques directly connect the cytoplasm of coupled cells, Cx43 channels also exist on their own as single membrane connexons or hemichannels that connect the cell cytoplasm to the extracellular milieu. Hemichannels are mostly active under pathological conditions, however, they have also been reported to participate in paracrine communication (Chever et al. 2014; D'Hondt et al. 2014). In the adult brain, Cx43 gap junction channels are highly expressed in astrocytes and to a lesser extent Cx30 and Cx26 (Giaume and Theis 2010). Gap junctions play a central role in organizing astrocytes into coupled cellular networks and facilitate communication between astrocytes, neurons and the vasculature (Giaume and Theis 2010).

Reduced levels of Cx43 expression result in detrimental outcome in stroke (Siushansian et al. 2001; Nakase et al. 2003b; Kozoriz et al. 2010; Le et al. 2014). Cx43 heterozygous null mice ($Cx43^{+/-}$) subjected to permanent middle cerebral artery occlusion (pMCAO) exhibited a significant increase in infarct volume, reduction in reactive astrocytes and an increase in apoptosis, 4 days after pMCAO (Siushansian et al. 2001; Nakase et al. 2003b). The data indicated that reduced astrocyte Cx43 coupling enhanced the neurodestructive effects of ischemia (Siushansian et al. 2001). A recent in vitro study showed that Cx43 coupling delayed neuronal death in an oxygen / glucose deprivation model (Shinotsuka et al. 2014). Taken together, Cx43 gap junctions may play a critical role in spatially buffering the apoptotic initiators and cytotoxic factors away from the peri-infarct zone (Nakase et al. 2004). In contrast, Cx43 hemichannel activity has been linked with inflammation and neurotoxicity by releasing inflammatory factors and glutamate during ischemic conditions (Retamal et al. 2007a; Orellana et al. 2009; Froger et al. 2010; Orellana et al. 2010; Kozoriz et al. 2013). Cx43 hemichannel blockers have been reported to alleviate cell injury in different pathological paradigms, including ischemia (Davidson et al. 2012; Maes et al. 2017; Willebrords et al. 2017). Recent developments in the field have introduced pharmacological agents that affect either Cx43 gap junction or hemichannel function (Ponsaerts et al. 2010; Desplantez et al. 2012; Skyschally et al. 2013; Wang et al. 2013; Chen et al. 2016).These pharmacological agents may be used as therapeutic factors in stroke as well as other brain injury paradigms. However, knowing the therapeutic window to administer treatment is critical for clinical applications of these drugs.

Using a well-established and widely-used stroke model (Chiang et al. 2011), which causes damage primarily to the sensory region of the parietal cortex, we sought to characterize the temporal and spatial expression profile of Cx43, with the goal of evaluating Cx43 as a potential therapeutic target within the treatment window for pMCAO. Visualization was achieved using histological stains, and semi-quantification by Western blotting of protein isolated from the ischemic and contralateral cortex. To correlate the extent of cell death with the Cx43 expression profile, we characterized the acute infarct region using a variety of well-validated methods. Emerging evidence suggests astrocytes are viable therapeutic targets as neuronal health is correlated with astrocytic health, which in turn is dependent on Cx43 channel activity (Barreto et al. 2011).

Materials and methods

Mice and surgery

This study was carried out in accordance with the recommendations of the Canadian Council on Animal Care through the Animal Care Committee of the University of British Columbia. The protocol was approved by the Animal Care Committee of the University of British Columbia.

Wildtype C57Bl/6 mice from the Jackson laboratory (Bar Harbor, USA) aged 7–9 months were used. Surgery was performed according to previously described procedures (Freitas-Andrade et al. 2017); mice were anesthetized with sodium pentobarbital (65 mg/Kg i.p.) and given an opiate (Buprenorphine, 0.1 mg/Kg) and a local analgesic (Bupivacaine, 0.1 ml at 0.25%) was given at incision site prior to surgery. Each animal was placed on a water heated pad and body temperature was maintained at 37 °C monitored with a rectal probe during surgery and recovery. The head was held securely in place using a stereotaxic frame (David Kopf Instruments, USA). With the aid of a dissecting microscope (Hund Wetzlar, Germany), a skin incision was made on the right side of the head from the anterior of the ear towards the corner of the eye horizontally and from the corner of the eye vertically 5 mm. The squamosal bone was exposed by gently pulling back the temporal muscle. Using a battery-powered micro drill (Dremel, Canada), a small hole was made ~2 mm in diameter on the skull bone to remove dura and expose the middle cerebral artery (MCA). The MCA was then cauterized

above and below the rhinal fissure using an electronic coagulator (Codman & Shurtleff Inc., USA) and the MCA was cut with micro scissors to ensure reperfusion did not occur. The skin incision was closed with sutures and mice were given a 1 ml subcutaneous bolus of lactate Ringer's solution. If any animal bled from the cauterized ends of the MCA, the animal was removed from the study and euthanized. Animals were given free access to food and water.

Brain extraction and sectioning

At the appropriate time-point, mice were anesthetized using a lethal dose of sodium pentobarbital (120 mg/Kg i.p.) and transcardially perfused with phosphate-buffered saline (PBS) followed by 10% Formalin for immunofluorescent labeling, thionin and Fuoro-Jade C staining or perfused with only PBS for the Western Blot analysis. Formalin fixed brains were cryoprotected in 30% sucrose and embedded in Optimal Cutting Temperature (OCT) Compound (Tissue-Tek®). The PBS perfused brains were immediately frozen in OCT on dry ice. Coronal sections were cut, using a cryostat microtome (Thermo-Scientific®, Microm HM 525), at 10 μm thickness for immunofluorescent labeling and Fluoro-Jade C staining and 20 μm thickness for Western blot analysis and thionin staining. Sections were then stored immediately at −20 ° C.

Immunofluorescent labeling

Immunofluorescent labeling was performed as previously described (Theodoric et al. 2012) on brain tissue collected at 30 min, 1 h, 2 h, 3 h, 6 h, 12 h, 24 h and 4-days after pMCAO. Sections 10 μm in thickness were rinsed in PBS, blocked with 2% bovine serum albumin (BSA) with 0.3% Triton X-100 in PBS for 1 h. Next, the sections were incubated overnight with primary antibodies: 1 in 200 anti-Cx43 raised in mouse (Sigma-Aldrich, Canada) and 1 in 100 anti-glial fibrillary acidic protein (GFAP) raised in rabbit (Sigma-Aldrich, Canada); or 1 in 400 anti-Cx43 raised in rabbit (Sigma-Aldrich, Canada) and 1 in 200 anti-MAP2 raised in mouse (Sigma-Aldrich, Canada) in 1% BSA with 0.3% Triton X-100 in PBS. Following removal of the primary antibody and three 10-min rinses with PBS, sections were incubated with Alexa Fluor secondary antibodies (Invitrogen, Canada) 1 in 500 for 1 h. Sections were then mounted with ProLong Gold antifade reagent with 4′,6-diamidino-2-phenylindole ([DAPI], Molecular Probes, USA).

Fluoro-Jade C staining

Fluoro-Jade C (Biosensis®: Catalog No: TR-100-FJ) was used to stain 10 μm formaldehyde-fixed sections at 30 min, 1 h, 2 h, 3 h, and 6 h to label degenerating neurons (Schmued et al. 2005), following the manufacturer's Ready-to-Dilute™ Fluoro-Jade® C Staining Protocol. In short, 10 μm thick fixed sections were dried in an incubator at 55 ° C to improve adhesion before placing slides in a Copland jar containing solution consisting of 9 parts 70% ethanol and 1 part NaOH solution from the kit for 5 min. The slides were then placed in 70% ethanol for 2 min, followed by distilled water for 2 min. Following this, slides were transferred to a solution containing 9 parts distilled water and 1 part KMnO4 from the kit for 10 min, then rinsed in distilled water for 2 min before being incubated for 10 min in the dark with a solution of 8 parts distilled water, 1 part Fluoro-Jade C solution from the kit, and 1 part DAPI solution from the kit. The slides were then washed 3 times, a minute each in distilled water and dried in an incubator at 55 ° C for approximately 10 min. Dry slides were cleared in xylene for approximately 2 min before coverslipping with CytoSeal™ XYL (Richard-Allan Scientific™, Thermo Scientific).

Thionin staining

To assess infarct damage, 20-μm-thick brain sections from mice subjected to pMCAO for 30 min, 1 h, 2 h, 6 h, 24 h and 4-days were collected every 200 μm and mounted sequentially on glass microscope slides. Sections were stained with 0.125% thionin (Fisher Scientific, Canada) solution as previously described (Kozoriz et al. 2010). Images of thionin-stained sections were captured using an EPSON Perfection V500 Photo scanner.

Protein isolation and western blot analysis

Protein samples were extracted from brain tissue sections from mice at 30 min, 1 h, 2 h, 3 h, and 6 h after pMCAO as previously described (Sadler et al. 2009; Freitas-Andrade et al. 2017). The region of infarct injury was identified visually and collected with a 27G needle (Becton Dickinson) under a dissecting microscope. On the contralateral side of each section, a symmetric area was also collected. Fresh-frozen tissue from eight 20 μm thick sections for each time point was combined into one Eppendorf tube per side containing 100 μL of radioimmunoprecipitation assay (RIPA) buffer with phosphatase inhibitor and protease inhibitor (Sigma-Aldrich, Canada). The mixture was vortexed for 10 s and sonicated for 30 s, and then centrifuged at 10000 G (Sigma 3-18 K Centrifuge). Protein determination and Western blot assay procedures were modified from previously established procedures (Freitas-Andrade et al. 2008). Briefly, protein concentrations were first determined by a bicinchoninic acid assay (Pierce, USA) and 15 μg of protein was denatured in protein loading buffer for 5 min at 100 ° C. Proteins were resolved by sodium dodecyl sulfate-polyacrylamide gel electrophoresis with a 15% gel and separated proteins were transferred to polyvinylidene difluoride membrane. Membranes were blocked by a 1 h room

temperature incubation with Tris-buffered saline with Tween 20 (TBS-T) [20 mM Tris-buffer at pH 8.0 and 150 mM NaCl with 0.1% Tween 20] with 5% skim milk. After blocking, membranes were incubated overnight at 4 ° C with primary antibodies against either rabbit anti-Cx43 C-terminal region (Sigma-Aldrich, Canada) or mouse anti-γ-tubulin (Sigma-Aldrich, Canada) diluted 1/5000 in TBS-T containing 1% skim milk. Membranes were subsequently washed with TBS-T and incubated with 1/5000 secondary antibody conjugated with horseradish peroxidase (Vector Laboratories Inc., USA) in TBS-T containing 5% skim milk. Finally, membranes were washed with TBS-T and immunoreactive proteins were visualized using chemiluminescent solution (Super Signal West Pico, Pierce Biotechnology Inc., USA) according to the manufacturer's instructions.

Data collection and analysis

Imaging of immunohistochemical sections was done using confocal microscopy (Leica DMI6000), taking tile scans of half-brains at 20× magnification. Western blots were scanned in using an EPSON Perfection V500 Photo scanner and intensities were analyzed using the ImageJ gel analysis plugin to find the slope under the intensity curve. The Fluoro-Jade C micrographs were captured using a Ziess Axioplan Fluorescent microscope using a 16X objective. For Western blots, the sample size was $n = 4$ and statistical analysis was performed using Kruskal-Wallis One Way Analysis of Variance on Ranks.

Results

Thionin staining indicates infarct after 1 h of pMCAO

Histological thionin staining was performed on brain tissue sections to visualize infarct progression in mice subjected to pMCAO at different time-points. While 30 min of pMCAO did not show obvious changes in thionin staining, we observed decreased thionin staining after 1 h and 2 h of pMCAO within the cortical region generally affected by this type of stroke model (Cechetto et al. 1989; Siushansian et al. 2001; Nakase et al. 2003b; Kozoriz et al. 2010; Freitas-Andrade et al. 2017) (indicated by thick black arrows in Fig. 1). After 6 h of pMCAO, an obvious decrease in thionin staining was observed within the affected cortical area (Fig. 1). In addition, vasodilation was also observed at the 6 h time point,

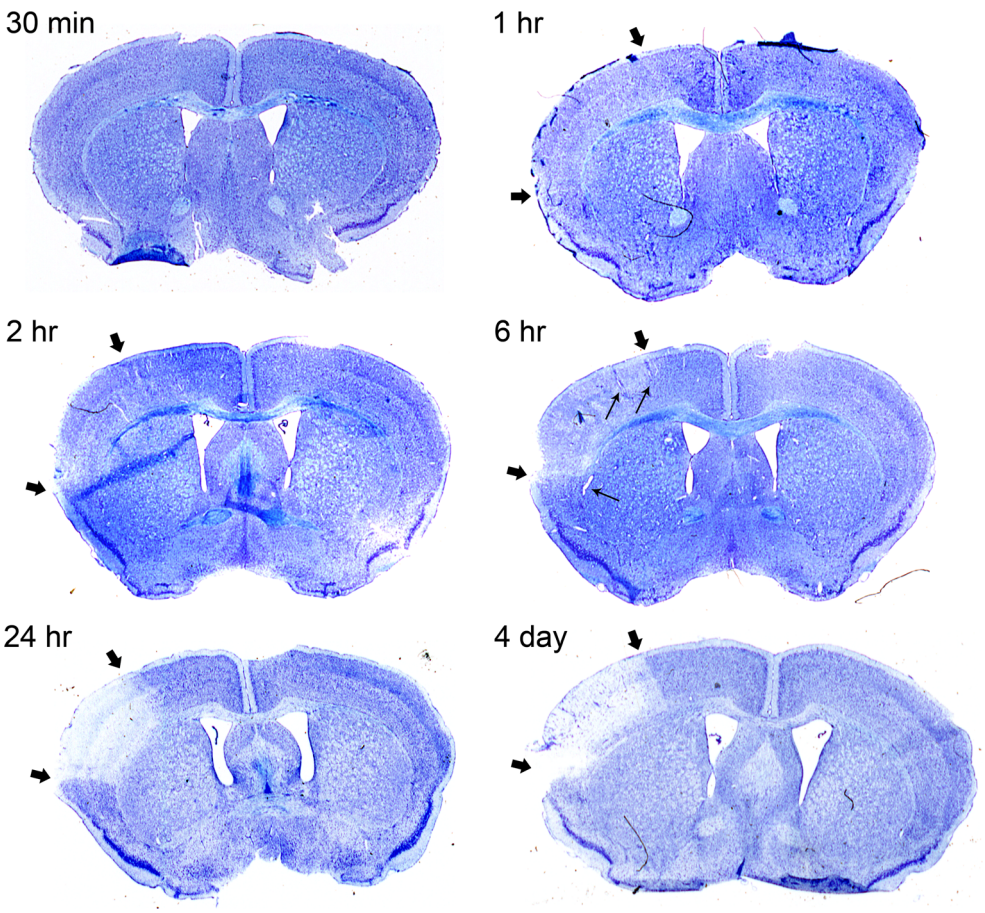

Fig. 1 Thionin staining timeline delineates damaged regions. Permanent MCAO was performed on mice to induce stroke on the left side of shown sections, as revealed by the decreased intensity of thionin staining in the infarct region. Brains were perfused after 30 min, 1 h, 2 h, 6 h, 24 h and 4 days after pMCAO and subsequently stained with thionin. Representative sections show a time-dependent decrease in staining intensity of the ischemic brain region starting at 1 h. The infarct region is demarcated by thick black arrows. The black arrows and corpus callosum indicate the boundaries of the region typically affected by pMCAO. This region is typically restricted to the cortex and does not extend into the striatum. Thin black arrows indicate dilated blood vessels in 6 h image

suggesting vascular responses to tissue hypoxia (indicated by thin black arrowheads in Fig. 1). After 24 h of pMCAO, very little thionin staining within the affected cortical area was observed and this did not change after a prolonged time-point of 4-days, indicating dead infarct tissue (Fig. 1).

Western analysis shows Cx43 upregulation at 2 h post-pMCAO

Cx43 upregulation is known to occur due to reactive astrocytes 4 days following pMCAO (for example, Nakase et al. 2003b). At this time, the central infarct region is entirely devoid of thionin staining, due to irreversible cell death (Fig. 1, 4-days post-pMCAO). To evaluate Cx43 expression before the onset of cell death, western blots were performed on protein isolated from brain tissue extracts from the ipsilateral region affected by pMCAO, as well as the contralateral region, within the first 6 h after pMCAO. While Cx43 protein levels were similar 30 min and 1 h after pMCAO, they were significantly higher in samples from the ipsilateral side 2 h and 3 h after pMCAO (Fig. 2a, b). However, after 6 h of pMCAO Cx43 levels were significantly reduced compared to the 30 min time-point (Fig. 2a, b). This decrease may be a result of the significant cell death occurring after 6 h of pMCAO, instead of an actual regulated decrease in Cx43 expression levels.

Bands of different sizes can be seen corresponding to phosphorylation isoforms of Cx43 (Solan and Lampe 2005, 2009). However, we were unable to reliably detect significant changes in the level of phosphorylated Cx43 isoforms, at various time-points, possibly due to phosphatases induced in injured cells.

Immunofluorescence shows Cx43 upregulation within 1 h post-pMCAO

We performed Cx43 immunofluorescence tissue staining to investigate spatial distribution and confirm the Western blot Cx43 expression analysis, up to 24 h post-pMCAO. Consistent with our Western blot data, increased Cx43 immunoreactivity was observed around the damaged region (dorsal to the cauterization site, white arrow head) starting at 1 h, with an increase in both fluorescence intensity and tissue area at 2 and 3 h after pMCAO, compared to 30 min post-pMCAO (Fig. 3). After 6 h of pMCAO, small "islands" (indicated by white traces) with little Cx43 immunoreactivity were observed, indicating the ischemic core (Fig. 3). The small infarct cores were surrounded by bright Cx43 staining in the peri-infarct area (Fig. 3). This may represent "mini-infarct cores" surrounded by "mini-penumbras" as previously reported (del Zoppo et al. 2011). The ischemic core, devoid of Cx43 staining, increased in size by 24 h post-pMCAO and was surrounded by Cx43-positive punctate staining in the peri-infarct zone (Fig. 3). In contrast, Cx43 immunostaining in

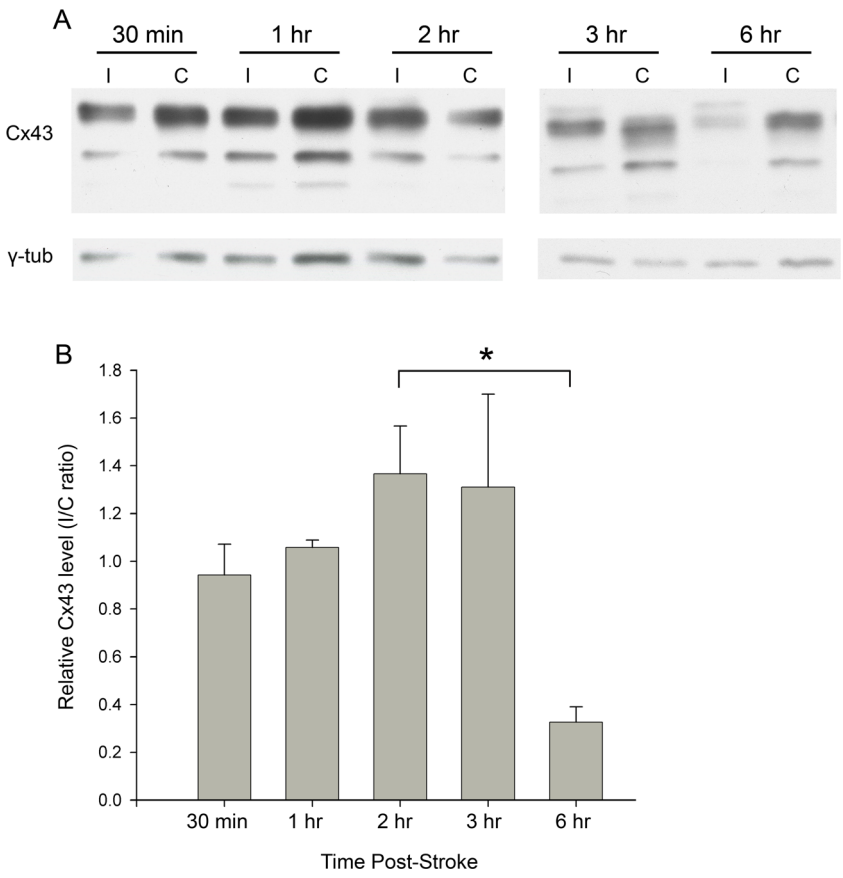

Fig. 2 Western blot analysis shows pattern of Cx43 expression in cerebral tissue acutely following stroke. Mice underwent pMCAO and were perfused after 30 min, 1 h, 2 h, 3 h, and 6 h. The area impacted by pMCAO on the ischemic side ("I"), as well as the mirrored area on the contralateral side ("C"), was removed and permeabilized; these samples were run on blots shown in (A). Intensity of Cx43 bands was measured and normalized against γ-tubulin; these values are plotted as a ratio of I/C on the y-axis in (B). Sample size: $n = 4$. Statistical analysis was performed using Kruskal-Wallis One Way Analysis of Variance on Ranks

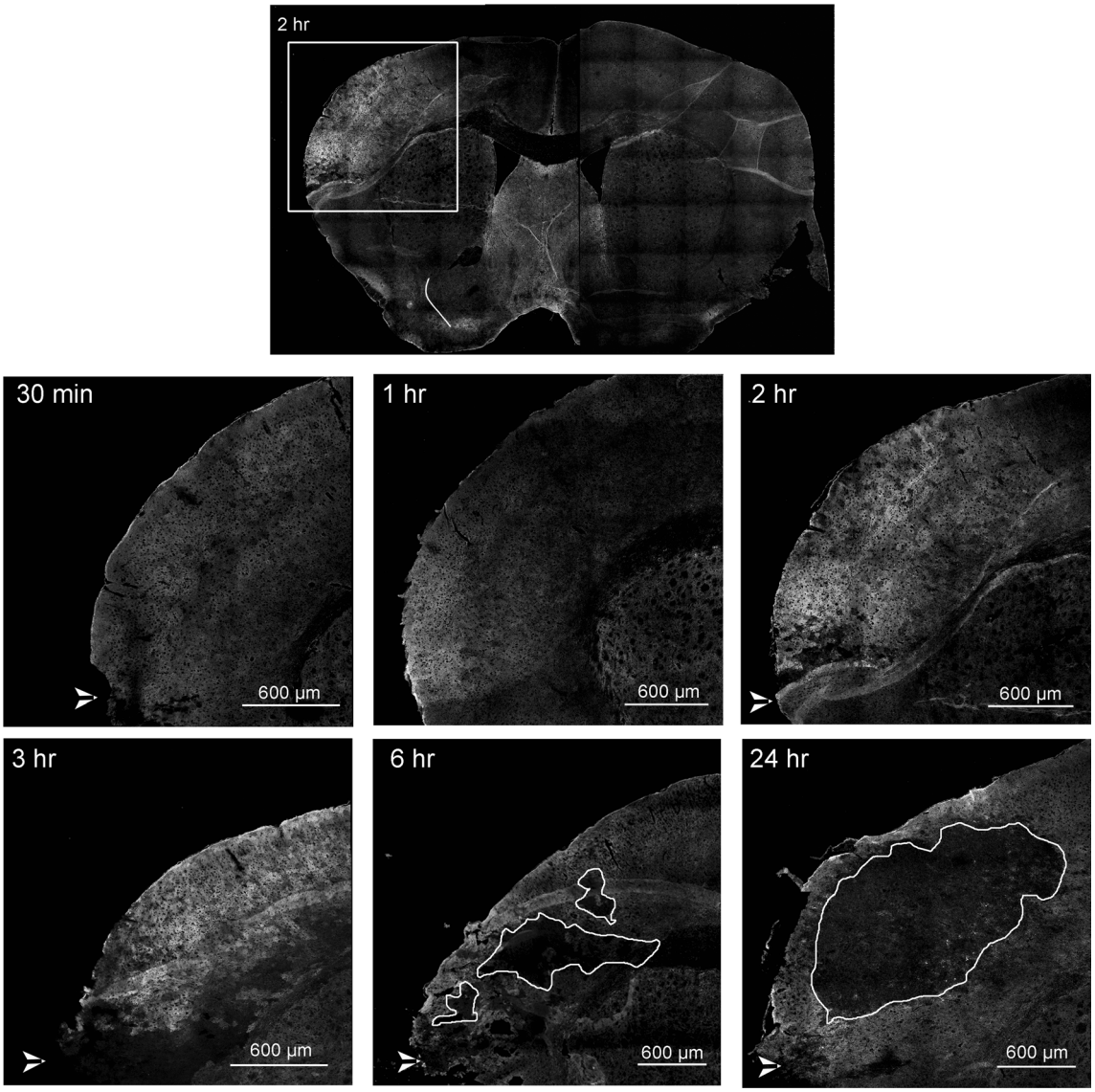

Fig. 3 Overview timeline of stroke regions. Fluorescent immunohistochemical staining of Cx43 on mouse coronal brain sections. The box area in the upper image shows the region of the brain typically affected by right hemisphere pMCAO; subsequent images are enlarged in the lower figures. Increased Cx43 immunoreactivity is evident starting at 1 h, peaking between 2 h to 3 h, and exhibiting an area of no staining in the infarct core starting at 6 h which continued to grow at 24 h, with intense Cx43 staining in the peri-infarct zone. White arrowheads in the bottom left of these images indicate the cauterization point. White line delineates the infarct core at 6 and 24 hrs

the contralateral non-ischemic cortex showed characteristic punctate staining, which did not change at any of the time-points investigated; a representative image showing both ipsilateral and contralateral cortex is shown in Fig. 3 (top micrograph). Sections shown are anterior sections since these regions are most impacted by pMCAO.

Fluoro-Jade staining reveals increasing cell degeneration starting at 1 h

To examine whether the region of low Cx43 immunoreactivity correlates to dead and damaged cells, Fluoro-Jade C staining was performed on fixed tissue (Fig. 4). While 30 min after pMCAO did not show any Fluoro-Jade positive cells, at 1 h post-pMCAO, faint Fluoro-Jade positive cells could be seen in cells dorsal to the site of cauterization, delineating an area of damage in the sensory region of the parietal cortex, with little staining beyond the corpus callosum (Fig. 4). After 2 h of pMCAO, Fluoro-Jade positive cells were brighter and extended further to the primary somatosensory region (Fig. 4). After 6 h of pMCAO, Fluoro-Jade positive cells were markedly brighter with a damaged region encompassing the primary somatosensory area (Fig. 4). Similar to Fig. 1 thionin staining, an increased vasodilation was observed after 6 h of pMCAO, indicated by white arrows (Fig. 4). For ease of visualization, magnified images of the punctate staining are shown.

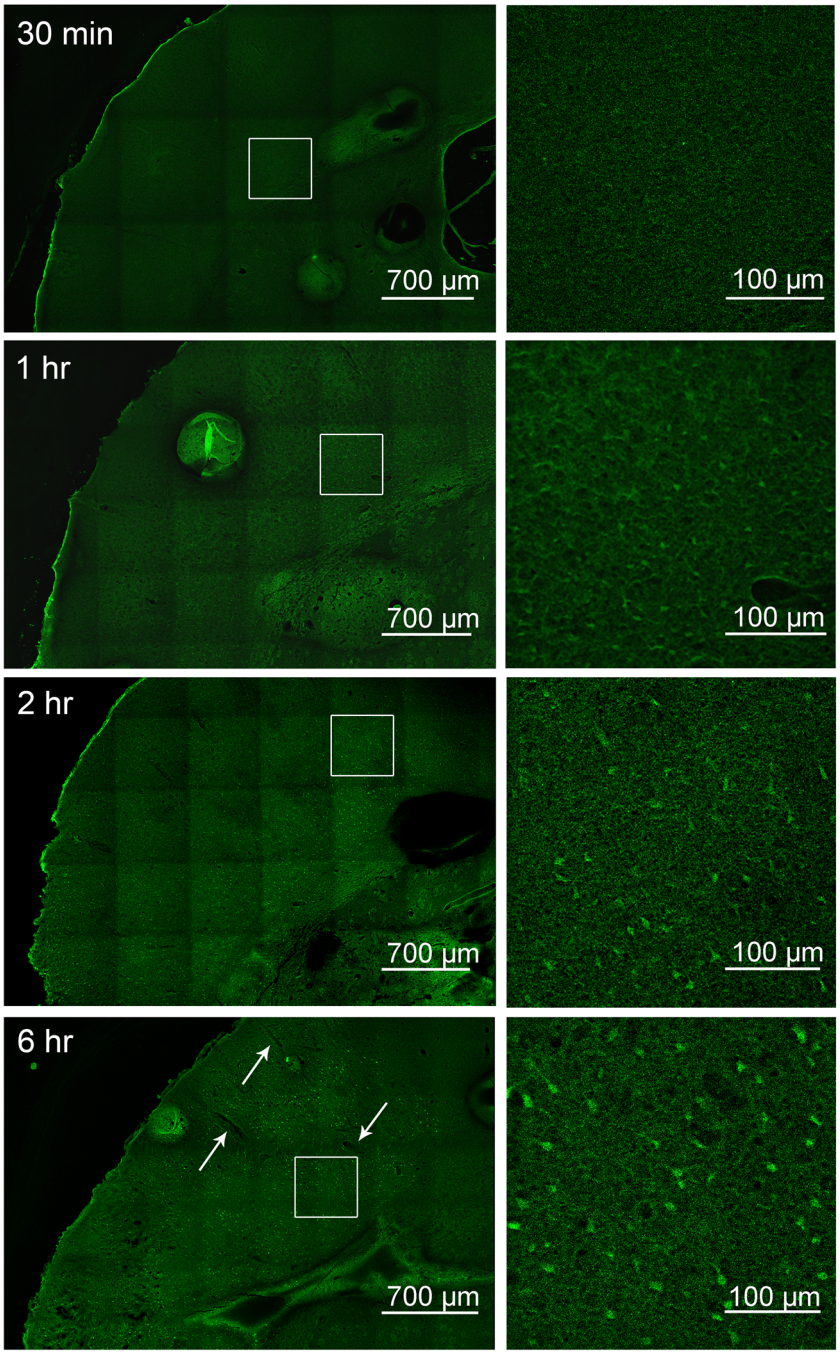

Fig. 4 Fluoro-Jade C staining indicates time-dependent increase in neuronal degeneration starting at 1 h post pMCAO. Brain sections of mice at time points of 30 min, 1 h, 2 h, and 6 h following pMCAO were stained with Fluoro-Jade C. The white squares in the left images outline the area which is magnified in the respective right images; Fluoro-Jade staining is evident starting at 1 h and increases in size and intensity with time. Images shown are representative from 3 experiments

MAP2 staining is decreased near the area of damage

Fluoro-Jade staining indicated that dead cells were present after 1 h of pMCAO, however, the cell type(s) affected are not distinguished using this method (Damjanac et al. 2007). To determine whether cell death indicated by Fluoro-Jade staining is neuronal, MAP2 (neuronal dendrite marker) was used to delineate acute brain injury resulting from neuronal death (Dawson and Hallenbeck 1996). In addition, co-immunostaining with Cx43 antibody was performed to determine the spatial expression of Cx43 relative to injured neurons. In our experiment, MAP2 staining at 30 min shows characteristic radial morphology in cortical regions within the infarct side, indistinguishable from the contralateral side (data not shown). At 30 min post-pMCAO, Cx43 punctate staining was stereotypically evenly distributed throughout the cortical brain area (Fig. 5). After 1 h of pMCAO, some disruption of MAP2-positive neurites was observed dorsal to the cauterized area, with slight blebbing, indicating microtubule dysregulation

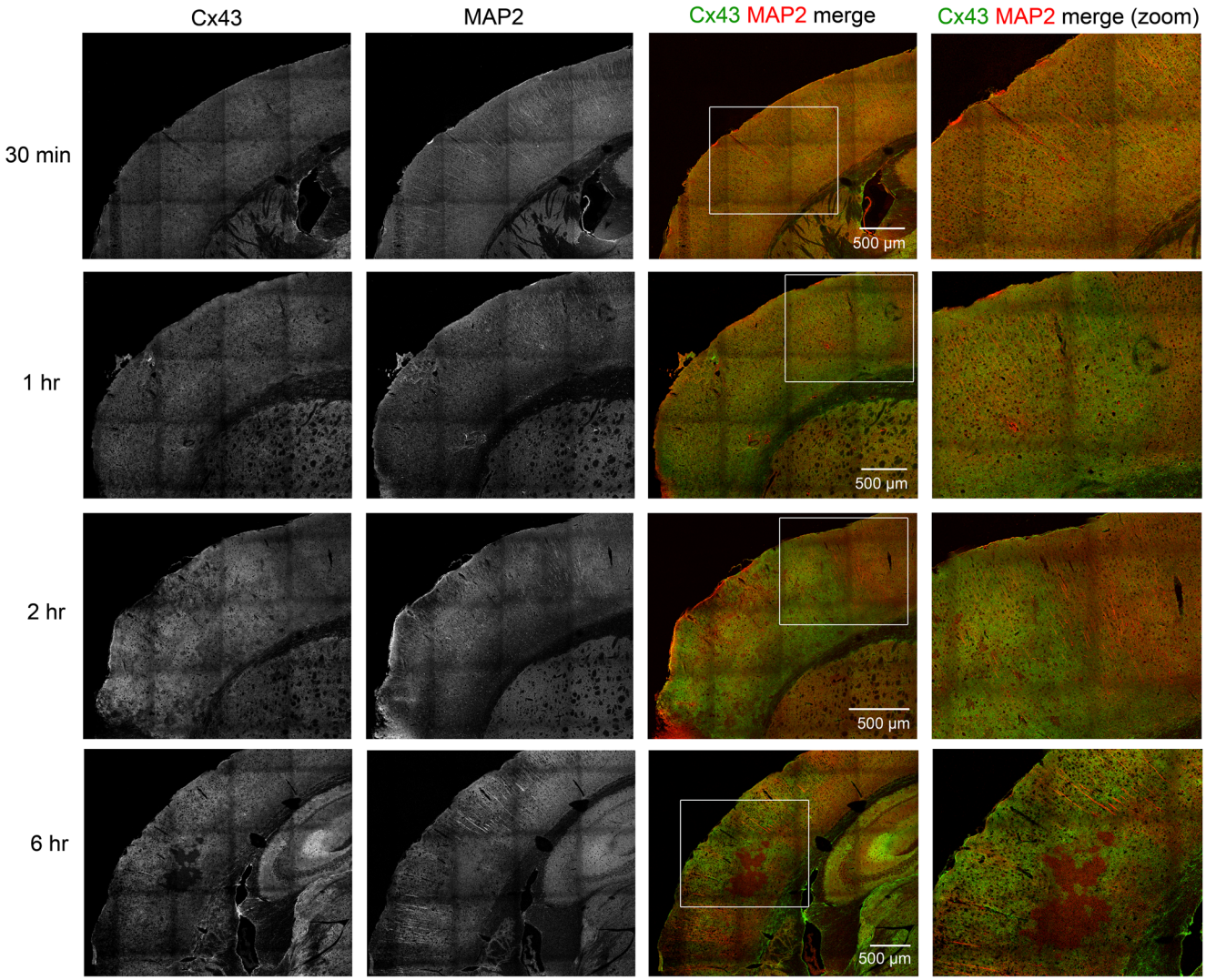

Fig. 5 Cx43 and MAP2 co-staining shows increased Cx43 immunoreactivity coinciding with decreased MAP2. Mice underwent pMCAO and were perfused after 30 min, 1 h, 2 h, and 6 h. Sections were stained for Cx43 and MAP2; a general time-dependent increase in Cx43 expression coinciding with decreased MAP2 staining in the impacted area. Boxed areas in the third column of images are magnified in the respective micrographs on the right

(Fig. 5). An increase in Cx43 immunoreactivity was observed at 1 h post-pMCAO within the somatosensory area affected by the stroke (Fig. 5). After 2 h of pMCAO, a decrease of MAP2 positive cells were more evident (Fig. 5). In contrast, an increase in Cx43 immunoreactivity was observed after 2 h of pMCAO, along with areas where Cx43 staining was not detected (Fig. 5). After 6 h of pMCAO, a larger area of MAP2 staining paucity was apparent (Fig. 5). Similarly, while Cx43 immunoreactivity was further increased in some areas, a larger region of Cx43 negative staining was also observed within the infarct (Fig. 5). This is consistent with the hypothesis that the mini-penumbras are consumed by the expanding mini-infarct cores over time, to generate a lesion that is ultimately homogenous and can grow into the surrounding injured tissue (del Zoppo et al. 2011).

Upregulation of Cx43 precedes GFAP increase in astrocytes

We previously reported that reactive astrocytes express increased levels of GFAP after 4 days of pMCAO (Nakase et al. 2003b; Kozoriz et al. 2010). Similarly, Cx43 expression levels are upregulated in reactive astrocytes in various brain pathologies including brain ischemia and epilepsy (Fonseca et al. 2002; Nakase et al. 2006; Cronin et al. 2008; Kozoriz et al. 2010; Theodoric et al. 2012). To determine whether Cx43 is an early marker of reactive astrocytes, we co-stained brain sections with Cx43 and GFAP after 3 h and 4-days pMCAO. Consistent with previous reports (Nakase et al. 2003b; Kozoriz et al. 2010), we observed upregulation and colocalization of Cx43 and GFAP at the peri-infarct region 4 days after pMCAO (Fig. 6). Interestingly, while Cx43 was

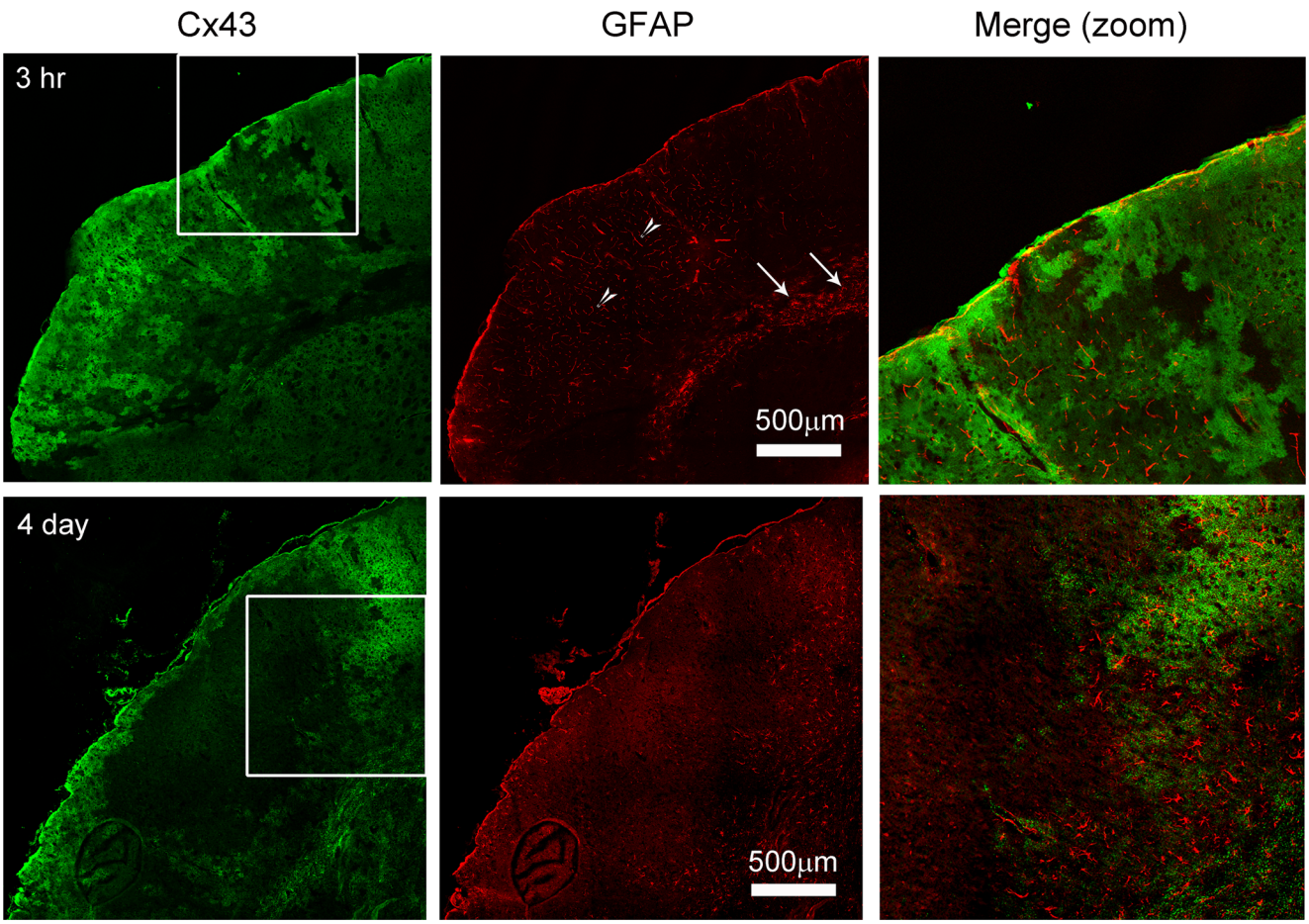

Fig. 6 Upregulation of Cx43 precedes GFAP in the infarct region. Mice underwent pMCAO and were perfused after 3 h and 4 days. Sections were stained for Rabbit anti-Cx43 and mouse anti-GFAP. Cx43 expression preceded increased GFAP at 3 h after pMCAO and colocalized with GFAP after 4-days post-pMCAO. GFAP is an established marker for reactive astrocytes, which is observed in Day 4. At 3 h post-stroke, staining that positive for GFAP is indicated in the striatum (arrows); GFAP staining in the blood vessels in the infarct region (arrowheads) is due to cross-reactivity of the secondary anti-mouse antibody due to the presence of mouse IgG from the leakage of vasculature during acute phase post-pMCAO

upregulated within the somatosensory area affected by the infarct after 3 h of pMCAO, no obvious GFAP astrocytic staining was observed within this region (Fig. 6). It should be noted, however, that the GFAP positive cells observed within the corpus callosum (white arrows) were not dependent on pMCAO, as they were also detected in the contralateral hemisphere. We also observed staining that corresponded to microvessels in the cortical region (white arrow heads) (Fig. 6). We suspected the staining was probably due to penetration of mouse IgG, from a compromised blood brain barrier in the acute phase within hours after pMCAO.

Discussion

We report here that Cx43 protein levels increase within the first 6 h of pMCAO in the cortical tissue affected by ischemia. Consistent with our previous findings (Siushansian et al. 2001; Nakase et al. 2003b; Kozoriz et al. 2010; Freitas-Andrade et al. 2017), Cx43 expression was still detected, in the peri-infarct zone, 4-days after pMCAO. This suggests that Cx43 may play a critical role in the evolving infarct over several days after ischemic injury. Indeed, we recently detected Cx43 expression in the peri-infarct zone up to 21-days after stroke (Freitas-Andrade et al., submitted). The data also indicates that Cx43 may be an early marker for reactive astrocytes, since Cx43 immunodetection preceded GFAP immunofluorescence, and Cx43 spatial expression was predominantly centered around injured or dying neurons in the infarcted tissue. Taken together, these findings and previous work by ourselves and others underscore Cx43 as a key player in the vulnerable and dynamic ischemic tissue and places Cx43 as a possible target for new therapeutic avenues of investigation.

Thionin is typically used to delineate infarct size (as described in (Nakase et al. 2003a)) as it stains for Nissl bodies, staining intensity is thus decreased with damage. Conversely, Fluoro-Jade is an anionic substance that stains degenerating neurons (Schmued et al. 2005) but also other cell types

including astrocytes (Damjanac et al. 2007). Similarly, MAP2 is known to serve as a reliable marker for acute brain injury from focal ischemia starting at 1 h (Dawson and Hallenbeck 1996). MAP2 is primarily associated with neurons; specifically, it is highly enriched in dendrites of neurons (Caceres et al. 1986). In this study, all three markers indicated ischemia-induced cell-stress beginning at 1 h and 2 h after pMCAO. Thionin staining was noticeably reduced 1 and 2 h after pMCAO, within the vulnerable ischemic area of the brain. The area delineated by decreased thionin staining largely did not change, since there was no obvious difference between the size of the affected region at 1 and 2 h versus 4 days after pMCAO. Similarly, both markers, Fluoro-Jade and MAP2, indicated cell damage evident at 1 and 2 h after pMCAO, compared to 30 min time-point. Cx43 protein expression was significantly increased after 2 and 3 h after pMCAO, measured by Western blot, indicating that astrocytes were responsive to perhaps both exposure to hypoxia and/or injured neurons within the ischemic brain tissue. During the first 2 h after brain ischemia a substantial proportion of astrocytes and neurons are still viable (Yoshimoto and Siesjo 1999; Anderson et al. 2003). Within this time window of infarct core expansion, any intervention that is able to restore normal blood flow or protect injured neurons is likely to reduce the final infarct volume (Hossmann 2012). However, little – if any –beneficial effects will occur if intervention is applied after 3 h post-ischemia (Hossmann 2012).

The effects of prolonged ischemia were evident at the 6 h time-point. Noticeable cell death and viable tissue loss were observed in the infarct core as well as marked vasodilation. Small areas devoid of MAP2 and thionin staining were observed and an increase in Fluoro-Jade positive cells was detected. Cx43 protein expression was also absent within the expanding infarct core which may have contributed to the significant decrease in Cx43 expression, measured by Western blot. Interestingly, the Cx43 immunostaining pattern demonstrated increased immunoreactivity surrounding small infarct cores. The Cx43 staining pattern shown here supports the model proposed by del Zoppo et al. 2011, suggesting that the core of ischemic injury develops heterogeneously, and with time coalesces dynamically into a homogenous core (del Zoppo et al. 2011). We show that at 6 h of pMCAO, pockets of injury that lacked Cx43 staining may indicate "mini-infarct cores" which were surrounded by "mini-penumbras" that stain heavily for Cx43. These mini-penumbras are then consumed by the expanding mini-cores that ultimately generates a lesion that is homogeneous, which we observe at 24 h and 4 days post-pMCAO with Cx43 staining. Therefore, Cx43 is potentially a useful early marker to delineate and investigate the progression of the mini-infarct cores proposed by del Zoppo.

Cx43 is upregulated in astrocytes under various brain pathologies (Siushansian et al. 2001; Fonseca et al. 2002; Nakase and Naus 2004; Cronin et al. 2008; Kozoriz et al. 2010; Theodoric et al. 2012); under these conditions, activation of astrocytes resulted in enhanced Cx43 expression in a period of days and/or weeks after the initial injury. In contrast, little is known regarding the temporal expression of Cx43 within minutes or hours after injury. Generally, there is a spatial temporal correlation between Cx43 and GFAP expression for the period between 3 to15 days post injury (Nakase et al. 2006; Kozoriz et al. 2010; Theodoric et al. 2012). In contrast to 4 day post-stroke where Cx43 and GFAP are upregulated in the peri-infarct region, we did not observe the filamentous GFAP staining at 3 h post stroke, suggesting that Cx43 upregulation in the infarct region may be a marker of early astrocyte reactivity, while GFAP is a 'late' maker of reactive astrocytes. Others have shown in astrocyte cultures, that an increase in extracellular glutamate and K^+ is correlated with an increase in Cx43 coupling (Enkvist and McCarthy 1994). This might reflect an adaptation of the astrocytic interstitial homeostasis control system for increasing the astrocytic dissipation of glutamate and K^+ from areas where their concentrations are elevated (Anderson et al. 2003). Similarly, the increased expression of Cx43 shown in both Western blot and immunofluorescence at 2 h of pMCAO may be an attempt by astrocytes to dissipate the toxic substrates accumulating in the infarct core.

In this study, we examined the spatial-temporal changes in Cx43 expression in the acute period following ischemic stroke using immunohistochemistry and Western blot analysis, with the overarching goal of exploring the possibility that Cx43 may be a viable therapeutic target. Indeed, others have shown that after an ischemic insult, astrocytic gap junctions in the core become internalized, while they remain intact at the penumbra (Li et al. 1998), suggesting that Cx43 is available for pharmaceutical manipulation in the vulnerable yet salvageable peri-infarct zone. While we have shown that Cx43 expression is affected by ischemia in the early stages of stroke, whether Cx43 is functioning as a hemichannel or gap junction during this time remains to be seen. In vitro hemichannel assays have found maximal Cx43 hemichannel activity 1 h following scratch damage, mediating secondary cellular injury (Rovegno et al. 2015). Opening of hemichannels, indicated by increased activity, can result in secretion of toxic substances such as ATP and glutamate into the ECM, exacerbating damage and increasing the lesioned area. At the same time gap junction coupling may also be occurring, transferring molecules between cells which may be detrimental or protective possibly depending on the proportion of damaged versus healthy cells (Meier and Rosenkranz 2014). In this case, it would be possible to target gap junctions with a widely used channel blocker, such as carbenoxolone (Tamura et al. 2011). However, given that gap junctions are believed to mediate long-term protection while transient hemichannel activity regulates acute damage (Retamal et al. 2007b), hemichannels may be better targets. Several molecules that target either hemichannel or gap junction function of Cx43 are available

(Yoon et al. 2010a, b; Davidson et al. 2012; Abudara et al. 2014). We have shown that targeting Cx43 hemichannels using hamichannel blocker Gap19 (Abudara et al. 2014) within 2 h after pMCAO, results in significant neuronal protection from stroke (Freitas-Andrade et al., submitted).

In conclusion, a large body of research has demonstrated the intricate and complex molecular cascades that contribute to cell death after stroke. However, the successful translation of experimental results into clinical application remains lacking. Many contributing factors for these failures have been reported (Lo et al. 2003; Sena et al. 2007). One such critical factor is the failure to appreciate the timing or window of opportunity in administering the drug to the appropriate molecular target. In light of this, the goal of our study is to characterize the temporal and spatial expression of Cx43 in a model of permanent focal cerebral ischemia, in order to establish a framework for future, clinically relevant, translational experiments.

Acknowledgements This study was funded through a grant from the Canadian Institutes of Health Research (CIHR) to CCN and WCS, and a CIHR Team Grant (R1478A47) on "Vascular Cognitive Impairment: Animal Models of Co-morbidity." MFA was supported by a fellowship from the Heart and Stroke Foundation of Canada. CCN holds a Canada Research Chair.

References

Abudara V, Bechberger J, Freitas-Andrade M, De Bock M, Wang N, Bultynck G, Naus CC, Leybaert L, Giaume C (2014) The connexin43 mimetic peptide Gap19 inhibits hemichannels without altering gap junctional communication in astrocytes. Front Cell Neurosci 8:306

Anderson MF, Blomstrand F, Blomstrand C, Eriksson PS, Nilsson M (2003) Astrocytes and stroke: networking for survival? Neurochem Res 28:293–305

Barreto G, White RE, Ouyang Y, Xu L, Giffard RG (2011) Astrocytes: targets for neuroprotection in stroke. Cent Nerv Syst Agents Med Chem 11:164–173

Broussalis E, Killer M, McCoy M, Harrer A, Trinka E, Kraus J (2012) Current therapies in ischemic stroke. Part a. Recent developments in acute stroke treatment and in stroke prevention. Drug Discov Today 17:296–309

Caceres A, Banker GA, Binder L (1986) Immunocytochemical localization of tubulin and microtubule-associated protein 2 during the development of hippocampal neurons in culture. J Neurosci 6:714–722

Cechetto DF, Wilson JX, Smith KE, Wolski D, Silver MD, Hachinski VC (1989) Autonomic and myocardial changes in middle cerebral artery occlusion: stroke models in the rat. Brain Res 502:296–305

Chen Q, Boire A, Jin X, Valiente M, Er EE, Lopez-Soto A, Jacob LS, Patwa R, Shah H, Xu K, Cross JR, Massague J (2016) Carcinoma-astrocyte gap junctions promote brain metastasis by cGAMP transfer. Nature 533:493–498

Chever O, Lee CY, Rouach N (2014) Astroglial connexin43 hemichannels tune basal excitatory synaptic transmission. J Neurosci 34: 11228–11232

Chiang T, Messing RO, Chou WH (2011) Mouse model of middle cerebral artery occlusion. J Vis Exp 13(48):e2761

Cronin M, Anderson PN, Cook JE, Green CR, Becker DL (2008) Blocking connexin43 expression reduces inflammation and improves functional recovery after spinal cord injury. Mol Cell Neurosci 39:152–160

Damjanac M, Rioux Bilan A, Barrier L, Pontcharraud R, Anne C, Hugon J, Page G (2007) Fluoro-jade B staining as useful tool to identify activated microglia and astrocytes in a mouse transgenic model of Alzheimer's disease. Brain Res 1128:40–49

Davidson JO, Green CR, Nicholson LF, O'Carroll SJ, Fraser M, Bennet L, Gunn AJ (2012) Connexin hemichannel blockade improves outcomes in a model of fetal ischemia. Ann Neurol 71:121–132

Dawson DA, Hallenbeck JM (1996) Acute focal ischemia-induced alterations in MAP2 immunostaining: description of temporal changes and utilization as a marker for volumetric assessment of acute brain injury. J Cereb Blood Flow Metab 16:170–174

del Zoppo GJ, Sharp FR, Heiss WD, Albers GW (2011) Heterogeneity in the penumbra. J Cereb Blood Flow Metab 31:1836–1851

Desplantez T, Verma V, Leybaert L, Evans WH, Weingart R (2012) Gap26, a connexin mimetic peptide, inhibits currents carried by connexin43 hemichannels and gap junction channels. Pharmacol Res 65:546–552

D'Hondt C, Iyyathurai J, Himpens B, Leybaert L, Bultynck G (2014) Cx43-hemichannel function and regulation in physiology and pathophysiology: insights from the bovine corneal endothelial cell system and beyond. Front Physiol 5:348

Enkvist MO, McCarthy KD (1994) Astroglial gap junction communication is increased by treatment with either glutamate or high K+ concentration. J Neurochem 62:489–495

Fonseca CG, Green CR, Nicholson LF (2002) Upregulation in astrocytic connexin 43 gap junction levels may exacerbate generalized seizures in mesial temporal lobe epilepsy. Brain Res 929:105–116

Freitas-Andrade M, Naus CC (2016) Astrocytes in neuroprotection and neurodegeneration: the role of connexin43 and pannexin1. Neuroscience 323:207–221

Freitas-Andrade M, Carmeliet P, Stanimirovic DB, Moreno M (2008) VEGFR-2-mediated increased proliferation and survival in response to oxygen and glucose deprivation in PlGF knockout astrocytes. J Neurochem 107:756–767

Freitas-Andrade M, Bechberger JF, MacVicar BA, Viau V, Naus CC (2017) Pannexin1 knockout and blockade reduces ischemic stroke injury in female, but not in male mice. Oncotarget 8:36973–36983

Froger N, Orellana JA, Calvo CF, Amigou E, Kozoriz MG, Naus CC, Saez JC, Giaume C (2010) Inhibition of cytokine-induced connexin43 hemichannel activity in astrocytes is neuroprotective. Mol Cell Neurosci 45:37–46

George PM, Steinberg GK (2015) Novel stroke therapeutics: unraveling stroke pathophysiology and its impact on clinical treatments. Neuron 87:297–309

Giaume C, Theis M (2010) Pharmacological and genetic approaches to study connexin-mediated channels in glial cells of the central nervous system. Brain Res Rev 63:160–176

Hossmann KA (2012) The two pathophysiologies of focal brain ischemia: implications for translational stroke research. J Cereb Blood Flow Metab 32:1310–1316

Kozoriz MG, Bechberger JF, Bechberger GR, Suen MW, Moreno AP, Maass K, Willecke K, Naus CC (2010) The connexin43 C-terminal region mediates neuroprotection during stroke. J Neuropathol Exp Neurol 69:196–206

Kozoriz MG, Lai S, Vega JL, Saez JC, Sin WC, Bechberger JF, Naus CC (2013) Cerebral ischemic injury is enhanced in a model of oculodentodigital dysplasia. Neuropharmacology 75:549–556

Lansberg MG, Bluhmki E, Thijs VN (2009) Efficacy and safety of tissue plasminogen activator 3 to 4.5 hours after acute ischemic stroke: a metaanalysis. Stroke 40:2438–2441

Le HT, Sin WC, Lozinsky S, Bechberger J, Vega JL, Guo XQ, Saez JC, Naus CC (2014) Gap junction intercellular communication mediated by connexin43 in astrocytes is essential for their resistance to oxidative stress. J Biol Chem 289:1345–1354

Li WE, Ochalski PA, Hertzberg EL, Nagy JI (1998) Immunorecognition, ultrastructure and phosphorylation status of astrocytic gap junctions and connexin43 in rat brain after cerebral focal ischaemia. Eur J Neurosci 10:2444–2463

Lo EH, Dalkara T, Moskowitz MA (2003) Mechanisms, challenges and opportunities in stroke. Nat Rev Neurosci 4:399–415

Maes M, Crespo Yanguas S, Willebrords J, Weemhoff JL, da Silva TC, Decrock E, Lebofsky M, Pereira IVA, Leybaert L, Farhood A, Jaeschke H, Cogliati B, Vinken M (2017) Connexin hemichannel inhibition reduces acetaminophen-induced liver injury in mice. Toxicol Lett 278:30–37

Meier C, Rosenkranz K (2014) Cx43 expression and function in the nervous system-implications for stem cell mediated regeneration. Front Physiol 5:106

Nakase T, Naus CC (2004) Gap junctions and neurological disorders of the central nervous system. Biochim Biophys Acta 1662:149–158

Nakase T, Fushiki S, Naus CC (2003a) Astrocytic gap junctions composed of connexin 43 reduce apoptotic neuronal damage in cerebral ischemia. Stroke 34:1987–1993

Nakase T, Fushiki S, Sohl G, Theis M, Willecke K, Naus CC (2003b) Neuroprotective role of astrocytic gap junctions in ischemic stroke. Cell Commun Adhes 10:413–417

Nakase T, Sohl G, Theis M, Willecke K, Naus CC (2004) Increased apoptosis and inflammation after focal brain ischemia in mice lacking connexin43 in astrocytes. Am J Pathol 164:2067–2075

Nakase T, Yoshida Y, Nagata K (2006) Enhanced connexin 43 immunoreactivity in penumbral areas in the human brain following ischemia. Glia 54:369–375

Orellana JA, Saez PJ, Shoji KF, Schalper KA, Palacios-Prado N, Velarde V, Giaume C, Bennett MV, Saez JC (2009) Modulation of brain hemichannels and gap junction channels by pro-inflammatory agents and their possible role in neurodegeneration. Antioxid Redox Signal 11:369–399

Orellana JA, Hernandez DE, Ezan P, Velarde V, Bennett MV, Giaume C, Saez JC (2010) Hypoxia in high glucose followed by reoxygenation in normal glucose reduces the viability of cortical astrocytes through increased permeability of connexin 43 hemichannels. Glia 58:329–343

Ponsaerts R, De Vuyst E, Retamal M, D'Hondt C, Vermeire D, Wang N, De Smedt H, Zimmermann P, Himpens B, Vereecke J, Leybaert L, Bultynck G (2010) Intramolecular loop/tail interactions are essential for connexin 43-hemichannel activity. FASEB J 24:4378–4395

Ramos-Cabrer P, Campos F, Sobrino T, Castillo J (2011) Targeting the ischemic penumbra. Stroke 42:S7–11

Retamal MA, Schalper KA, Shoji KF, Orellana JA, Bennett MV, Saez JC (2007a) Possible involvement of different connexin43 domains in plasma membrane permeabilization induced by ischemia-reperfusion. J Membr Biol 218:49–63

Retamal MA, Froger N, Palacios-Prado N, Ezan P, Saez PJ, Saez JC, Giaume C (2007b) Cx43 hemichannels and gap junction channels in astrocytes are regulated oppositely by proinflammatory cytokines released from activated microglia. J Neurosci 27:13781–13792

Rovegno M, Soto PA, Saez PJ, Naus CC, Saez JC, von Bernhardi R (2015) Connexin43 hemichannels mediate secondary cellular damage spread from the trauma zone to distal zones in astrocyte monolayers. Glia 63:1185–1199

Sadler TR, Khodavirdi AC, Hinton DR, Holschneider DP (2009) Snap-frozen brain tissue sections stored with desiccant at ambient laboratory conditions without chemical fixation are resistant to degradation for a minimum of 6 months. Appl Immunohistochem Mol Morphol 17:165–171

Schmued LC, Stowers CC, Scallet AC, Xu L (2005) Fluoro-jade C results in ultra high resolution and contrast labeling of degenerating neurons. Brain Res 1035:24–31

Sena E, van der Worp HB, Howells D, Macleod M (2007) How can we improve the pre-clinical development of drugs for stroke? Trends Neurosci 30:433–439

Shinotsuka T, Yasui M, Nuriya M (2014) Astrocytic gap junctional networks suppress cellular damage in an in vitro model of ischemia. Biochem Biophys Res Commun 444:171–176

Siushansian R, Bechberger JF, Cechetto DF, Hachinski VC, Naus CC (2001) Connexin43 null mutation increases infarct size after stroke. J Comp Neurol 440:387–394

Skyschally A, Walter B, Schultz Hansen R, Heusch G (2013) The antiarrhythmic dipeptide ZP1609 (danegaptide) when given at reperfusion reduces myocardial infarct size in pigs. Naunyn-Schmiedeberg's. Arch Pharm 386:383–391

Solan JL, Lampe PD (2005) Connexin phosphorylation as a regulatory event linked to gap junction channel assembly. Biochim Biophys Acta 1711:154–163

Solan JL, Lampe PD (2009) Connexin43 phosphorylation: structural changes and biological effects. Biochem J 419:261–272

Tamura K, Alessandri B, Heimann A, Kempski O (2011) The effect of a gap-junction blocker, carbenoxolone, on ischemic brain injury and cortical spreading depression. Neuroscience 194:262–271

Theodoric N, Bechberger JF, Naus CC, Sin WC (2012) Role of gap junction protein Connexin43 in astrogliosis induced by brain injury. PLoS One 7:e47311

Wang N et al (2013) Selective inhibition of Cx43 hemichannels by Gap19 and its impact on myocardial ischemia/reperfusion injury. Basic Res Cardiol 108:309

Willebrords J, Cogliati B, Pereira IVA, da Silva TC, Crespo Yanguas S, Maes M, Govoni VM, Lima A, Felisbino DA, Decrock E, Nogueira MS, de Castro IA, Leclercq I, Leybaert L, Rodrigues RM, Vinken M (2017) Inhibition of connexin hemichannels alleviates non-alcoholic steatohepatitis in mice. Sci Rep 7:8268

Yoon JJ, Green CR, O'Carroll SJ, Nicholson LF (2010a) Dose-dependent protective effect of connexin43 mimetic peptide against neurodegeneration in an ex vivo model of epileptiform lesion. Epilepsy Res 92:153–162

Yoon JJ, Nicholson LF, Feng SX, Vis JC, Green CR (2010b) A novel method of organotypic brain slice culture using connexin-specific antisense oligodeoxynucleotides to improve neuronal survival. Brain Res 1353:194–203

Yoshimoto T, Siesjo BK (1999) Posttreatment with the immunosuppressant cyclosporin a in transient focal ischemia. Brain Res 839:283–291